International Journal of Tropical Engineering and Computing
Vol. 1, No 1. June 2025, pp. 32~50
https://doi.org/10.60787/ijtec.vol1no1.34

Available online at https://ijtec.org.ng

Integrated Geophysical, Geochemical, and Geospatial Investigation of Leachate Migration at Otofure Dumpsite, Benin City, Nigeria

[1]Idowu Rudolph Ilaboya and [*2]Osahon Michael Enodiana

[1]Department of Civil Engineering, Faculty of Engineering, University of Benin, Benin City, Nigeria (Email: rudolph.ilaboya@uniben.edu, ORCID: https://orcid.org/0000-0002-8982-7404)
[2]Department of Civil Engineering, Faculty of Engineering, University of Benin, Benin City, Nigeria Email: michael.enodiana@eng.uniben.edu, ORCID: https://orcid.org/0009-0003-7450-579X)

***Correspondent Author**: michael.enodiana@eng.uniben.edu; **Tel**: +2348114322929*

Article Information

Article history: Received May 2025
Revised June 2025
Accepted June 2025
Published online July 2025

Citation: Ilaboya, I. R., & Enodiana, O. M. (2025). Integrated Geophysical, Geochemical, and Geospatial Investigation of Leachate Migration at Otofure Dumpsite, Benin City, Nigeria. International Journal of Tropical Engineering and Computing, 1(1), pp. 32~50. https://doi.org/10.60787/ijtec.vol1no1.34

Official Journal of Tropical Engineering and Computing Research Network (TREN Research Group) at the faculty of Engineering of Benson Idahosa University, Nigeria.

Abstract

Dumpsites situated in groundwater recharge zones pose serious threats to nearby shallow aquifers. In this study, the potential for groundwater contamination around the Otofure Dumpsite in Benin City, Edo State, was assessed to guide sustainable waste management practices. A geoelectrical survey using an ABEM SAS 300C Terrameter with a dipole-dipole configuration and Vertical Electrical Sounding (VES) was conducted to evaluate subsurface resistivity and delineate geological formations. Soil samples were analyzed using X-Ray Fluorescence (XRF) spectrometry to determine elemental composition, and spatial distribution maps were created using Inverse Distance Weighting (IDW) interpolation. Results showed that leachate migration was primarily limited to the top 10 meters of soil, restricted by an underlying impermeable clay layer. The XRF analysis revealed that heavy metal concentrations were below permissible limits, indicating limited soil contamination and minimal risk to deeper groundwater. These findings support informed decision-making for dumpsite siting and environmental monitoring in vulnerable recharge areas.

***Keywords**: Leachate transport; soil quality assessment; geoelectrical survey; groundwater contamination; Otofure dumpsite.*

Graphical Abstract

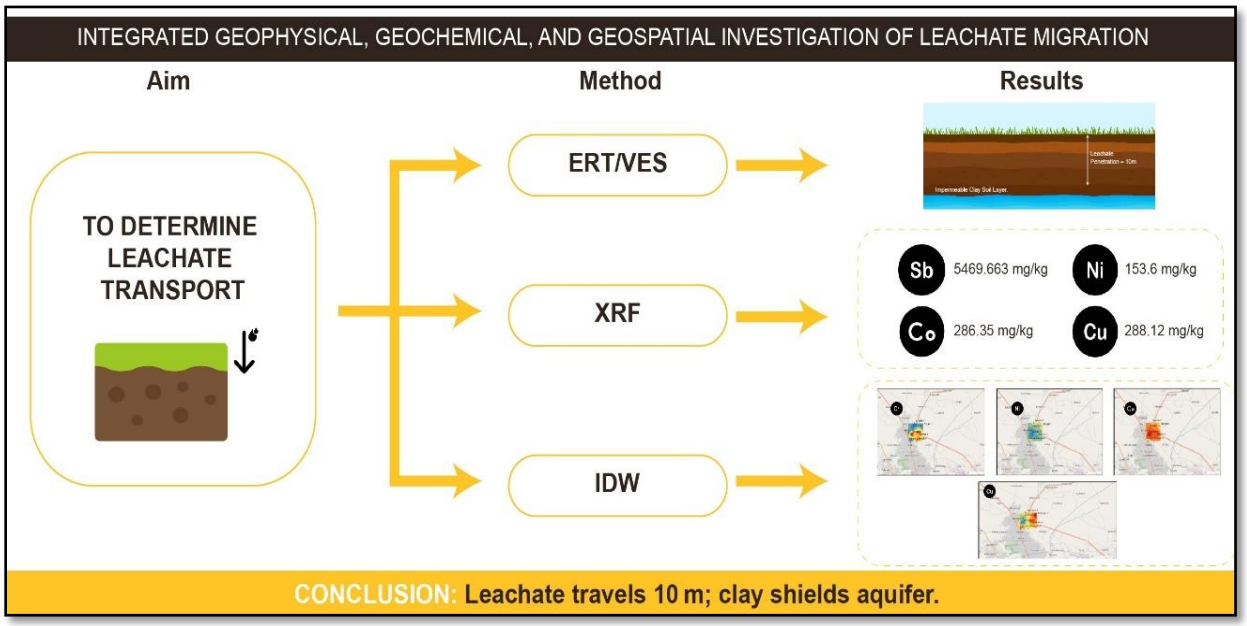

1.0 INTRODUCTION

Urban dumpsites often unregulated and improperly located pose serious threats to subsurface and surface water systems when situated near groundwater recharge zones. In low- and middle-income countries, weak environmental oversight exacerbates these risks, making such areas especially vulnerable to long-term health and socio-economic impacts. Leachate, the liquid product of waste decomposition, often mobilizes heavy metals (Pb, Cd, Fe, Zn) and organic pollutants, which percolate through soils into aquifers used for domestic and agricultural purposes. Ige et al. [1]

To effectively detect and delineate leachate plume migration, recent studies have emphasized integrated geophysical and hydro-chemical approaches. Electrical resistivity techniques, including Vertical Electrical Sounding (VES) and 2D imaging, remain fundamental due to their non-invasive and cost-effective nature. For example, Adeoye et al. [2] used VES and dipole-dipole profiling at the Ilokun dumpsite in Ado-Ekiti, Nigeria, revealing low resistivity zones (< 12 Ω·m) within fractured basement layers, consistent with contaminant plumes. Similarly, Olatunji & Fauzan [3] employed VLF-EM coupled with VES around the reclaimed Amoyo dumpsite and confirmed persistent leachate in shallow aquifers.

Hydro-chemical data support these geophysical findings. In the Aduramigba–Onibu-Eja Estate near Osogbo, Nigeria, elevated levels of nitrate (~74 mg/L), chloride (331 mg/L), sulfate (222 mg/L), and heavy metals (Pb, Zn, Cu, Ni) were detected alongside geophysical anomalies indicating leachate depths of 3.5–6 m. Ojo et al. [4]. Likewise, at the Oke Asunle dumpsite in Ile-Ife, combined resistivity and water chemistry assessments identified subsurface zones with low resistivity (15–47 Ω·m) and heavy metal concentrations (Cd, Fe, Pb) exceeding WHO limits. Joe-Ukairo and Oni [5].

Beyond point studies, broader-scale investigations highlight seasonal and spatial contamination patterns. In Lagos, monthly monitoring around the massive Olusosun landfill during 2020 revealed that heavy metals (Pb^{2+}, Ni^{+}, Mn^{2+}, Fe^{2+}, Cr^{6+}) and other parameters exceeded WHO thresholds more during the wet season, with water quality index shifting toward "unsuitable" in 12–18% of sampled wells. Ferreira et al. [6] Furthermore, geoelectrical modeling in southeastern Nigeria demonstrated the effectiveness of Electrical Resistivity Tomography (ERT) in mapping leachate plumes within fractured aquifers. These modeling approaches enhance interpretation of resistivity data by accounting for subsurface heterogeneity. Udosen. [7]

These studies, although provide valuable frameworks, many focus primarily on groundwater contamination without integrating detailed soil quality assessments or spatial modelling techniques like Inverse Distance Weighting (IDW). Moreover, localized studies in Edo State remain limited, particularly around the Otofure Dumpsite. This study addresses these gaps by conducting an integrated assessment of contaminant transport and soil quality degradation around the Otofure Dumpsite, Benin City. Using dipole-dipole geoelectrical survey, VES, and X-Ray Fluorescence

https://doi.org/10.60787/ijtec.vol1no1.34

(XRF) analysis, the study maps leachate flow paths, identifies subsurface geological controls, and evaluates the distribution of heavy metals in the soil. The incorporation of geospatial analysis further enhances the understanding of spatial variability in soil contamination. By providing a detailed and site-specific evaluation, this research contributes to improved environmental monitoring frameworks and offers practical insights for siting and managing future dumpsites in Nigeria and similar settings.

2.0 MATERIALS AND METHODS

2.1 Study Area

The study area is Otofure dumpsite located along Benin Ifon Road by Oluku Bridge, Benin City Edo State Nigeria. Benin City is located in the southern region of Nigeria. The City is a humid tropical urban settlement which comprises three Local Government Areas namely Egor, Ikpoba Okha and Oredo. It is located within latitudes 6020'N and 6058'N and longitudes 5035'E and 5041'E. It broadly occupies an area of approximately 112.552 sq km. It is the fourth largest city in Nigeria after Lagos, Kano and Ibadan with a total population of 1,782,000 as of 2021 (Benin City History and facts Encyclopedia Britannica). The weather is uncomfortably hot and humid year-round, and generally very dull, especially between July and September. Benin City experiences the highest amount of rainfall between the months of May – November, with the month of November topping the charts.

The dumpsite is located in Ovia North East Local Government areas of Edo state between Oluku and Iyowa community. The Otofure dumpsite is located in latitude 60 26′ 58.92″N and longitude 50 35′ 49.45″E near the bypass linking Benin - Lagos Road to Benin – Ekpoma road. It was converted from an old burrow pit for lateritic sand for construction. The dumpsite is managed by the Ministry of Environment anchored by Edo State Waste Management Board. The upland section of the dumpsite grows cassava, with many tiny shelters used by scavengers who collect recyclable goods for sale on the outskirts. Figure 1 is the study area map showing the location of the dumpsite

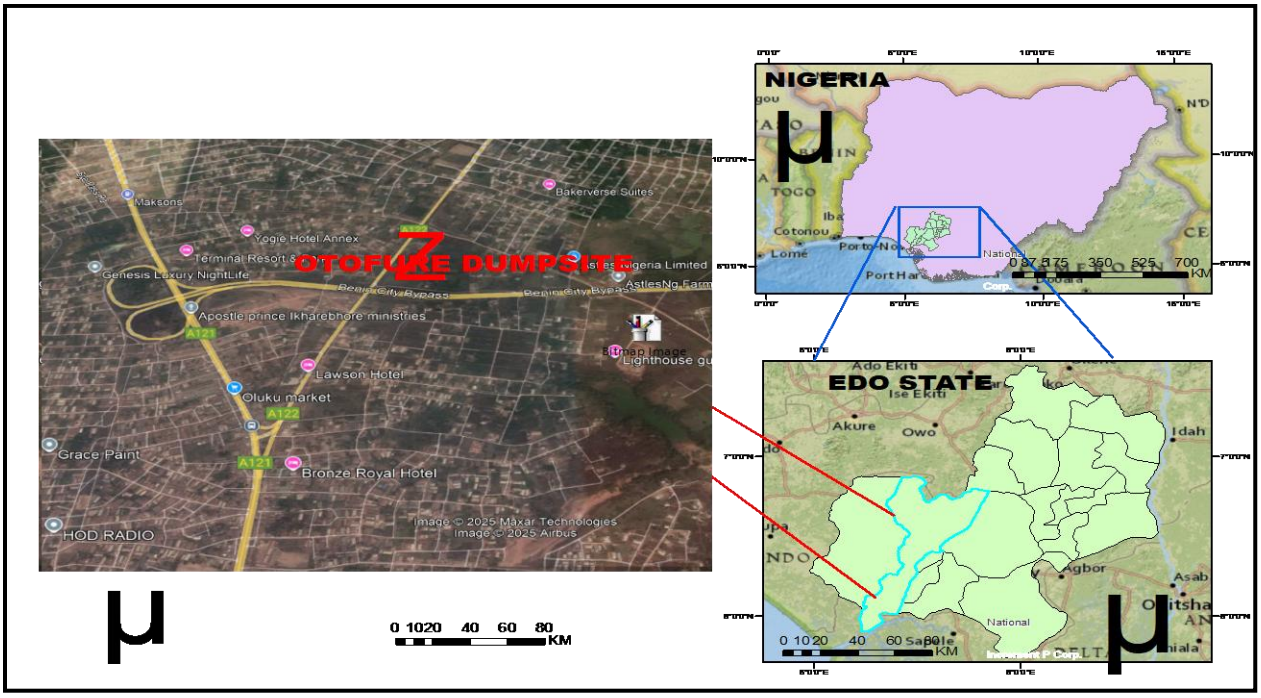

Figure 1: Map showing Otofure dumpsite in Oluku area of Benin City

2.2 Geophysical Investigation

The ABEM Terrameter SAS 300C, global positioning systems (GPS) for coordinate and elevation measurements, DIPRO application version 4.01 (iterative software programs for 2-D resistivity inversion), winRESIST software version 1.0 (a computer-assisted 1-D forward modeling tool), and Surfer Software program for contouring were utilized to conduct the VES and ERT resistivity survey around the dumpsite.

Electrical resistivity methods were employed to investigate subsurface conditions and delineate the extent

https://doi.org/10.60787/ijtec.vol1no1.34

of leachate-induced contamination around the dumpsite. The survey combined 1-D Vertical Electrical Sounding (VES) and 2-D Dipole–Dipole imaging to evaluate lithological layering and identify low-resistivity leachate plumes. Zaina et al. [8]

Two traverse lines (TR1 and TR2), were established for the 2-D resistivity imaging. Data acquisition used a Dipole–Dipole array with electrode spacing (a) of 10 meters and expansion factors (n) up to 5, allowing for adequate horizontal and vertical resolution. The VES data were acquired using the Schlumberger configuration at 8 stations spaced uniformly across the site.

Field implementation involved inserting four stainless steel electrodes into the ground to a depth of approximately 1 meter using a hand-held hammer. Electrodes were connected to the Terrameter with insulated copper cables. Voltage and current measurements were automatically logged and stored. All data were processed and inverted using DIPRO software, applying least-squares inversion to generate true resistivity models.

A direct current was introduced into the subsurface via the current electrodes (C1 and C2), while the potential electrodes (P1 and P2) measured the resulting voltage difference, as illustrated in Figure 2. The dipole-dipole array is one member of a family of arrays using dipoles (closely spaced electrode pairs) to measure the curvature of the potential field. If the separation between both pairs of electrodes is the same a, and the separation between the centers of the dipoles is restricted to a(n+1). USEPA [9]. The apparent resistivity is given as:

$$\rho_a = \pi a n(n+1)(n+2)\frac{\Delta V}{I} \quad (1)$$

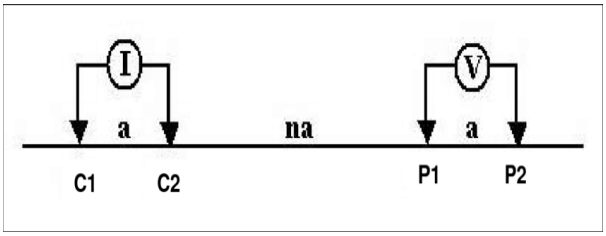

Figure 2: Dipole-dipole array configuration

The DIPRO software version 4.01 was used to process and invert the 2-D Dipole-Dipole data, generating two-dimensional resistivity profiles that were essential for analyzing subsurface characteristics and pinpointing potential zones of contamination. Additionally, eight (8) Vertical Electrical Sounding (VES) surveys were carried out using the Schlumberger electrode configuration, with a maximum current and voltage output of 2 amps and 600 volts, respectively. The resulting depth sounding curves from the VES points were interpreted quantitatively using winRESIST version 1.0, a 1-D forward modeling software that applies partial curve matching techniques to facilitate accurate data analysis. The data gotten from both transverses are shown in tables 1a - 1c and 2a – 2c below:

Table 1a: Geophysical Survey Data (Transverse 1)
Dipole-Dipole Array | P_2 Electrode Position: 30–70 m
Instrument: ABEM SAS 300 | Electrode Spacing: 10 m | Elevation: 113 m–109 m
Start Coordinates: 06°27'53.472"N, 05°36'2.514"E | End Coordinates: 06°27'48.486"N, 05°36'0.696"E

C1	C2	P1	P2	Geometric Factor (m)	Resistance (Ω)	Apparent Resistivity (Ω·m)
0	10	20	30	188.52	5.30	999.16
0	10	30	40	754.08	4.74	3574.34
0	10	40	50	1885.20	6.67	12574.28
0	10	50	60	3770.40	7.16	26996.06
0	10	60	70	6598.20	3.03	19992.55
10	20	30	40	188.52	1.883	354.98
10	20	40	50	754.08	0.42	316.71
10	20	50	60	1885.20	0.26	490.15
10	20	60	70	3770.40	0.197	742.77
10	20	70	80	6598.20	0.15	989.73
20	30	40	50	188.52	1.30	245.08
20	30	50	60	754.08	0.29	218.68
20	30	60	70	1885.20	1.39	2620.43
20	30	70	80	3770.40	0.007	26.39
20	30	80	90	6598.20	0.16	1055.71
30	40	50	60	188.52	1.94	365.73
30	40	60	70	754.08	0.63	475.07
30	40	70	80	1885.20	0.243	458.10
30	40	80	90	3770.40	0.08	301.63
30	40	90	100	6598.20	0.116	765.39
30	40	50	60	188.52	1.94	365.73
30	40	60	70	754.08	0.63	475.07
40	50	60	70	188.52	2.10	395.89
40	50	70	80	754.08	0.583	439.63
40	50	80	90	1885.20	0.23	433.60

https://doi.org/10.60787/ijtec.vol1no1.34

Table 1b: Geophysical Survey Data (Transverse 1)
Dipole-Dipole Array | P_2 Electrode Position: 80–140 m

C1	C2	P1	P2	Geometric Factor (m)	Resistance (Ω)	Apparent Resistivity (Ω·m)
40	50	90	100	3770.40	0.086	324.25
40	50	100	110	6598.20	2.24	14779.97
50	60	70	80	188.52	1.764	332549.28
50	60	80	90	754.08	0.75	565.56
50	60	90	100	1885.20	0.645	1215.95
50	60	100	110	3770.40	0.198	746.54
50	60	110	120	6598.20	0.106	699.41
60	70	80	90	188.52	1.50	282.78
60	70	90	100	754.08	0.235	177.21
60	70	100	110	1885.20	0.684	1289.48
60	70	110	120	3770.40	0.09	339.34
60	70	120	130	6598.20	0.09	593.84
70	80	90	100	188.52	1.246	234.90
70	80	100	110	754.08	0.322	242.81
70	80	110	120	1885.20	0.16	301.63
70	80	120	130	3770.40	0.07	263.93
70	80	130	140	6598.20	0.08	527.86
80	90	100	110	188.52	0.27	50.90
80	90	110	120	754.08	0.07	52.79
80	90	120	130	1885.20	0.11	207.37
80	90	130	140	3770.40	0.04	150.82
80	90	140	150	6598.20	0.06	395.89
90	100	110	120	188.52	0.24	45.24
90	100	120	130	754.08	0.23	173.44
90	100	130	140	1885.20	0.03	56.56

Table 1c: Geophysical Survey Data (Transverse 1)
Dipole-Dipole Array | P_2 Electrode Position: 150–180 m

C1	C2	P1	P2	Geometric Factor (m)	Resistance (Ω)	Apparent Resistivity (Ω·m)
90	100	150	160	6598.20	0.235	1550.58
100	110	120	130	188.52	0.20	37.70
100	110	130	140	754.08	0.11	82.95
100	110	140	150	1885.20	0.13	245.08
100	110	150	160	3770.40	0.20	754.08
100	110	160	170	6598.20	0.39	2573.30
110	120	130	140	188.52	1.79	337.45
110	120	140	150	754.08	0.29	218.68
110	120	150	160	1885.20	0.272	512.77
110	120	160	170	3770.40	0.20	754.08
110	120	170	180	6598.20	0.00	0.00
120	130	140	150	188.52	0.82	154.59
120	130	150	160	754.08	0.368	277.50
120	130	160	170	1885.20	0.08	150.82
130	140	150	160	188.52	0.801	151.13
130	140	160	170	754.08	0.345	260.00
130	140	170	180	1885.20	0.00	0.00
140	150	160	170	188.52	0.785	148.00

https://doi.org/10.60787/ijtec.vol1no1.34

Table 2a: Geophysical Survey Data (Transverse 2)
Dipole-Dipole Array | P_2 Electrode Position: 30–70 m
Instrument: ABEM SAS 300 | Electrode Spacing: 10 m | Elevation: 111 m–106 m
Start Coordinates: 06°27'53.916"N, 05°36'3.216"E | End Coordinates: 06°27'51.018"N, 05°36'8.352"E

C1	C2	P1	P2	Geometric Factor (m)	Resistance (Ω)	Apparent Resistivity (Ω·m)
0	10	20	30	188.52	4.92	927.5184
0	10	30	40	754.08	1.57	1183.9056
0	10	40	50	1885.2	0.72	1357.344
0	10	50	60	3770.4	0.275	1036.86
0	10	60	70	6598.2	0.23	1517.586
10	20	30	40	188.52	10.87	2049.2124
10	20	40	50	754.08	3.1	2337.648
10	20	50	60	1885.2	0.819	1543.9788
10	20	60	70	3770.4	0.57	2149.128
10	20	70	80	6598.2	0.37	2441.334
20	30	40	50	188.52	8.91	1679.7132
20	30	50	60	754.08	1.449	1092.66192
20	30	60	70	1885.2	0.83	1564.716
20	30	70	80	3770.4	0.5	1885.2
20	30	80	90	6598.2	0.39	2573.298
30	40	50	60	188.52	5.05	952.026
30	40	60	70	754.08	1.53	1153.7424
30	40	70	80	1885.2	0.69	1300.788
30	40	80	90	3770.4	0.53	1998.312
30	40	90	100	6598.2	0.25	1649.55
40	50	60	70	188.52	5.05	952.026
40	50	70	80	754.08	1.13	852.1104
40	50	80	90	1885.2	0.045	84.834

Table 2b: Geophysical Survey Data (Transverse 2)
Dipole-Dipole Array | P_2 Electrode Position: 80–140 m

C1	C2	P1	P2	Geometric Factor (m)	Resistance (Ω)	Apparent Resistivity (Ω·m)
40	50	90	100	3770.4	0.61	2299.944
40	50	100	110	6598.2	0.33	2177.406
50	60	70	80	188.52	4.25	801.21
50	60	80	90	754.08	1.342	1011.97536
50	60	90	100	1885.2	1.09	2054.868
50	60	100	110	3770.4	0.6	2262.24
50	60	110	120	6598.2	0.352	2322.5664
60	70	80	90	188.52	3.61	680.5572
60	70	90	100	754.08	1.51	1138.6608
60	70	100	110	1885.2	0.72	1357.344
60	70	110	120	3770.4	0.398	1500.6192
60	70	120	130	6598.2	0.23	1517.586
70	80	90	100	188.52	6.28	1183.9056
70	80	100	110	754.08	1.82	1372.4256
70	80	110	120	1885.2	0.634	1195.2168
70	80	120	130	3770.4	0.37	1395.048
70	80	130	140	6598.2	0.182	1200.8724
80	90	100	110	188.52	5.81	1095.3012
80	90	110	120	754.08	1.275	961.452
80	90	120	130	1885.2	0.58	1093.416
80	90	130	140	3770.4	0.229	863.4216
80	190	140	150	6598.2	0.22	1451.604
90	100	110	120	188.52	5.68	1070.7936
90	100	120	130	754.08	1.52	1146.2016
90	100	130	140	1885.2	0.574	1082.1048
90	100	140	150	3770.4	0.43	1621.272

https://doi.org/10.60787/ijtec.vol1no1.34

Table 2c: Geophysical Survey Data (Transverse 2)
Dipole-Dipole Array | P_2 Electrode Position: 150–230 m

C1	C2	P1	P2	Geometric Factor (m)	Resistance (Ω)	Apparent Resistivity (Ω·m)
90	100	150	160	6598.2	0.225	1484.595
100	110	120	130	188.52	4.79	903.0108
100	110	130	140	754.08	0.872	657.55776
100	110	140	150	1885.2	0.53	999.156
100	110	150	160	3770.4	0.17	640.968
100	110	160	170	6598.2	0.08	527.856
110	120	130	140	188.52	2.81	529.7412
110	120	140	150	754.08	0.7	527.856
110	120	150	160	1885.2	0.28	527.856
110	120	160	170	3770.4	0.209	788.0136
110	120	170	180	6598.2	0.141	930.3462
120	130	140	150	188.52	4.21	793.6692
120	130	150	160	754.08	0.9	678.672
120	130	160	170	1885.2	0.456	859.6512
120	130	170	180	3770.4	0.28	1055.712
120	130	180	190	6598.2	0.31	2045.442
130	140	150	160	188.52	1.8	339.336
130	140	160	170	754.08	0.591	445.66128
130	140	170	180	1885.2	0.32	603.264
130	140	180	190	3770.4	0.36	1357.344
130	140	190	200	6598.2	0	0
140	150	160	170	188.52	1.721	324.44292
140	150	170	180	754.08	0.79	595.7232
140	150	180	190	1885.2	0.73	1376.196
140	150	190	200	3770.4	0	0
140	150	200	210	6598.2	0	0
150	160	170	180	188.52	1.42	267.6984
150	160	180	190	754.08	0.89	671.1312
150	160	190	200	1885.2	0	0
150	160	200	210	3770.4	0	0
150	160	210	220	6598.2	0	0
160	170	180	190	188.52	2.57	484.4964
160	170	190	200	754.08	0	0
160	170	200	210	1885.2	0	0
160	170	210	220	3770.4	0	0
160	170	220	230	6598.2	0	0

https://doi.org/10.60787/ijtec.vol1no1.34

2.3 Soil Sample Collection, Pretreatment, Digestion, and Elemental Analysis

Soil samples were collected randomly from eight (8) georeferenced points around the dumpsite. At each sampling point, topsoil was collected to a depth of 15 cm using a stainless-steel auger. The quartering technique was employed to obtain representative samples from each location. This involved thoroughly mixing two or more subsamples from a given location to form a composite sample. The composite was then divided into four equal parts, and one quarter was further subdivided into four portions. One of these was selected as the representative sample for analysis. The representative soil samples were air-dried for 24–36 hours, crushed with a mortar and pestle, and sieved through a 2mm mesh to remove debris and ensure uniform particle size. The processed samples were then stored in labeled polythene bags for laboratory analysis.

For the elemental analysis of soil samples, a wet digestion method was used prior to X-ray fluorescence (XRF) spectrometry. One gram (1g) of each dried, homogenized sample was mixed with 10mL of a 1:1 HNO_3:H_2SO_4 solution in a 50mL conical flask. The mixture was heated to 95–100°C and refluxed for 15 minutes without boiling. After cooling in a desiccator, 5mL of concentrated nitric acid was added, and the solution was again refluxed for 35 minutes until brown fumes were observed. The sample was further heated to evaporate excess liquid and then cooled. Subsequently, 2mL of distilled water and 3mL of hydrogen peroxide were added to oxidize any remaining organic matter. The solution was reheated and, after cooling, 10mL of concentrated hydrochloric acid was added and heated for 2 minutes at 95–100°C.

Following digestion, the solution was filtered using Whatman No. 42 filter paper. The filtrate was analyzed using the SKYRAY EDXRF model EDX3600B spectrometer. This instrument, based on X-ray fluorescence (XRF) technology, is capable of detecting elements ranging from Sodium (Na, Z = 11) to Uranium (U, Z = 92). The spectrometer's operation involves four stages: initialization (calibration using a pure silver standard), selection of an appropriate working curve based on sample type, sample testing, and result transmission. This method ensures reliable identification and quantification of elemental composition within the soil samples. Table 3 below shows the heavy metal composition of the soil in mg/grams.

Table 3: Heavy Metals in Otofure Dumpsite *Metal composition unit: mg/grams*

ID	Sample 1	Sample 2	Sample 3	Sample 4	Sample 5	Sample 6	Sample 7	Sample 8
EASTING (m)	789742	787376	786788	788579	788870	787647	788105	787500
NORTHING (m)	716896	714356	715750	714365	715767	716565	717442	715523
ELEVATION (m)	101	101	101	108	105	104	112	114
Mg	0	0	0	0	0	0	0	0
Al	1.6991	1.7952	2.3412	1.9519	2.5162	2.3108	1.9834	2.3455
Si	9.013	10.3528	5.0089	3.9192	3.3785	3.7374	5.0352	3.0992
P	0.0303	0.0402	0.025	0.0349	0.0342	0.0296	0.0398	0.0223
K	0	0.1875	0.0003	0.0135	0.0454	0	0.0054	0.0015
Ca	0.0889	0.1732	0.0132	0.0157	0.0112	0.015	0.0127	0.044
Ti	0.0515	0	0.6015	1.0135	1.1264	1.2403	1.3044	1.1672
V	0	0.007	0	0.0041	0	0.0062	0	0
Cr	0	0	0	0.0107	0.0116	0	0	0.0142
Mn	0	0.0129	0	0.0283	0.0174	0.0307	0.2656	0.0845
Co	0.04	0.0199	0.0252	0.3457	0.4244	0.3658	0.1943	0.8755
Fe	3.4194	3.6933	6.4363	11.1423	14.9791	15.2562	10.5498	25.629
Ni	0.1783	0.177	0.1687	0.1499	0.1517	0.1484	0.1787	0.0761
Cu	0.3996	0.3612	0.3242	0.3024	0.3716	0.1593	0.3275	0.059
Zn	0.2642	0.2643	0.2132	0.2258	0.2259	0.2176	0.2181	0.1749
As	0	0	0	0	0	0	0	0
Pb	0.0208	0	0	0.0133	0.0248	0	0.021	0.0052
W	0.0594	0	0.0441	0.1227	0.1521	0	0.2738	0.0201
Au	0	0	0	0	0	0	0	0
Ag	0	0	0	0	0	0.0124	0.0394	0
Rb	0	0.0046	0.0005	0.0037	0	0.0025	0.0011	0.0013
Nb	0.0167	0	0.0073	0.0411	0	0.0857	0.0652	0.0473
Mo	0.389	0.2576	0.1247	0.3877	0.239	0.3051	0.2479	0.1503
Cd	0	0	0	0.0009	0	0	0	0
Sn	7.3749	6.747	6.9153	6.4608	5.8106	5.3255	6.0469	4.2382
Sb	6.2349	6.0664	6.3488	5.4325	5.2738	4.8516	5.5183	4.031

https://doi.org/10.60787/ijtec.vol1no1.34

3.0 RESULTS AND DISCUSSION

3.1 Geophysical Investigation

Resistivity data from transverse 1 were employed to generate the 2-D dipole-dipole profile maps presented in Figures 3 and 4

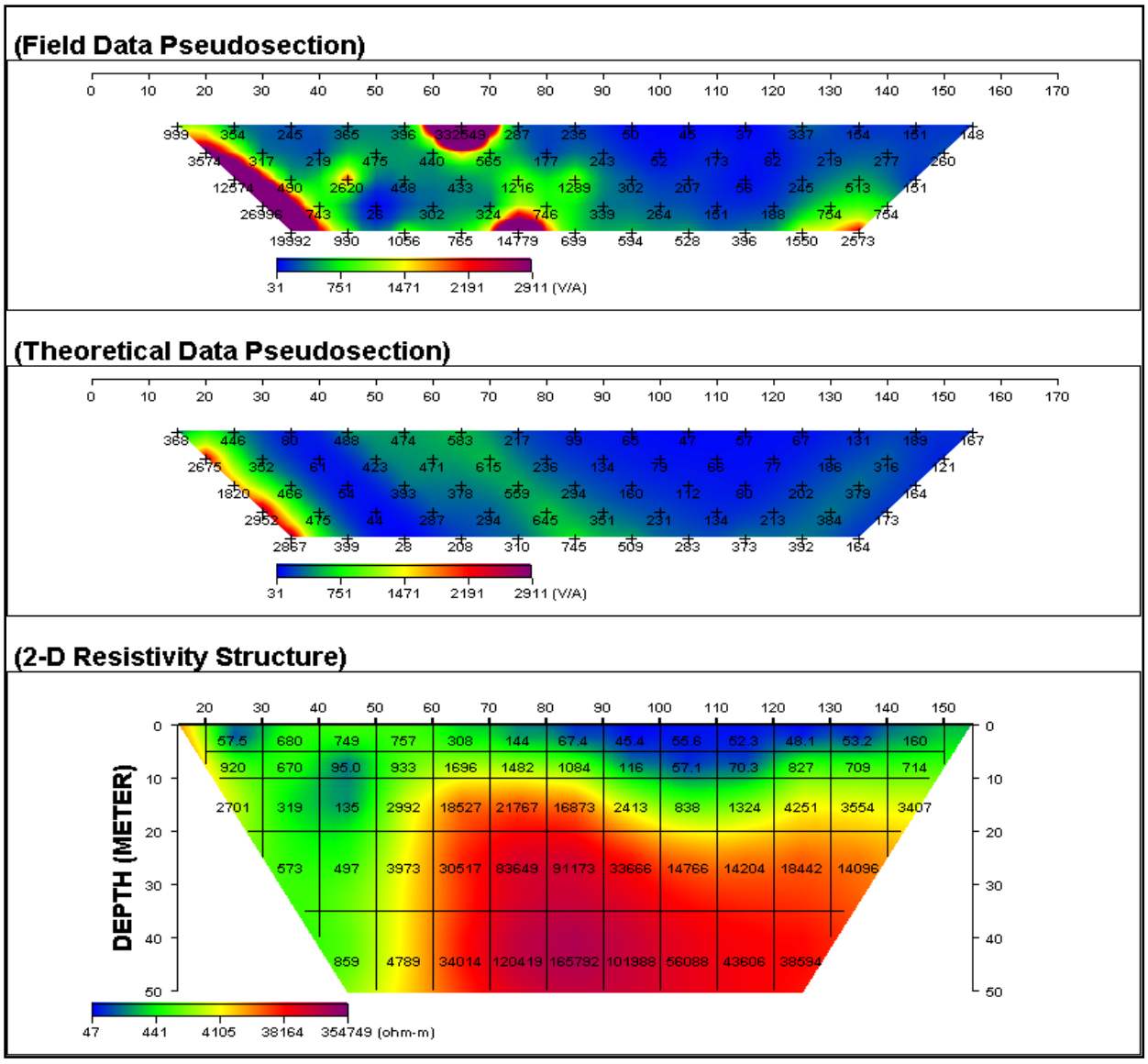

Figure 3: Dipro Inversion based on FEM Modelling

https://doi.org/10.60787/ijtec.vol1no1.34

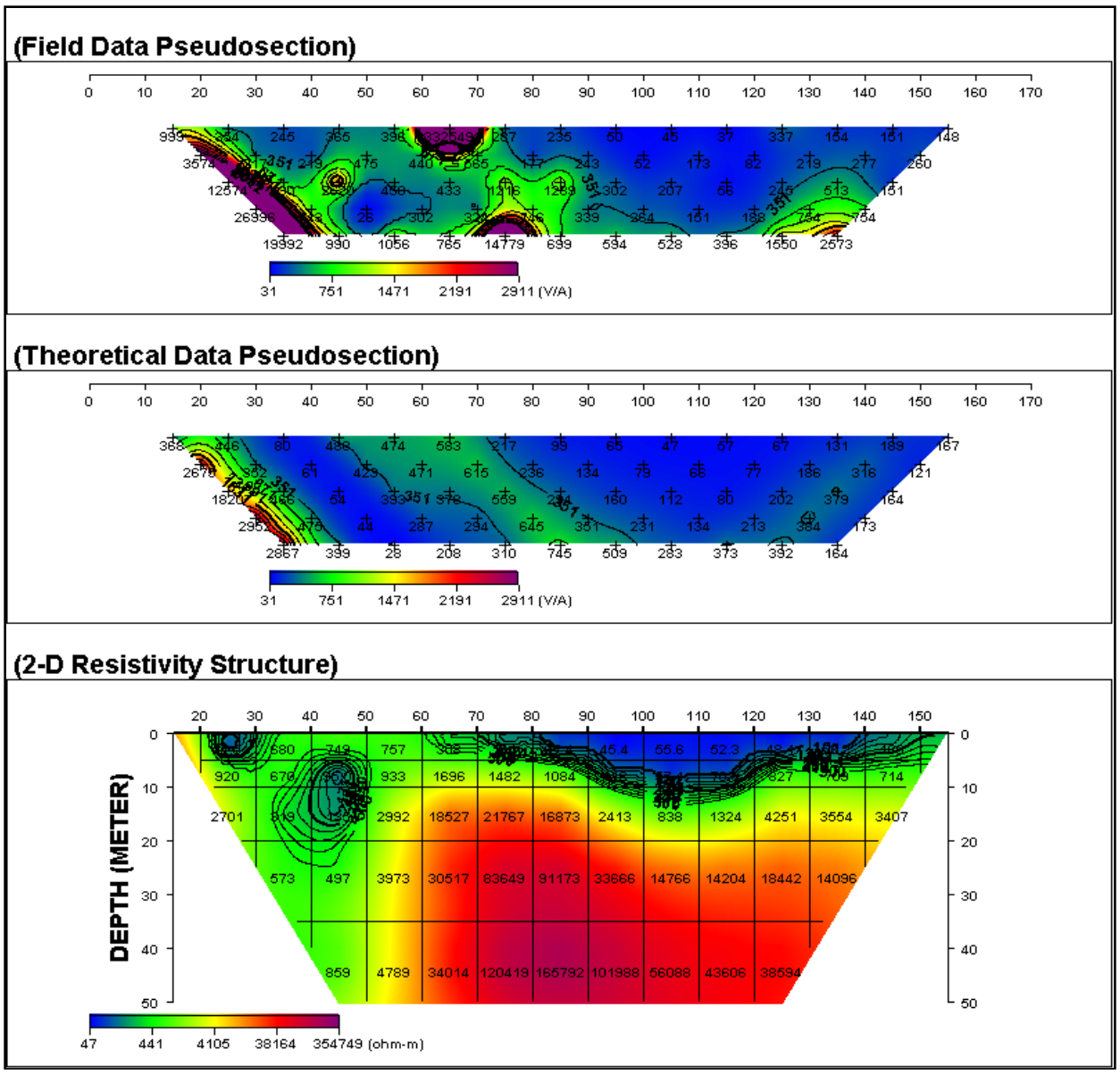

Figure 4: Dipro Inversion based on FEM Modeling with contours

The 2-D resistivity imaging along the first transverse line, as presented in Figures 3 and 4, reveals significant subsurface variations in resistivity that provide insights into the lithological composition and degree of contamination in the area. The resistivity values at the surface range from 57.5 Ωm to 116 Ωm and tend to increase with depth, indicating a progressive transition in subsurface materials and possibly a reduction in moisture or contaminant content.

At a horizontal distance of 20 to 30 meters and shallow depths of 0 to 5 meters, a notably low resistivity zone of 57.5 Ωm was detected, which is characteristic of a leachate-contaminated area. Similarly, at 70 to 145 meters horizontally and 0 to 10 meters in depth, resistivity values range from 45.4 Ωm to 116 Ωm, also indicating significant leachate infiltration in the topsoil. These low resistivity readings are associated with high moisture content and elevated concentrations of dissolved ions, typically found in leachate plumes. Further subsurface characterization reveals that between 40 and 50 meters horizontally and 10 to 20 meters depth, the resistivity ranges from 95 Ωm to 135 Ωm, suggesting a transition zone potentially influenced by partial contamination or moisture migration. However, the deeper penetration of leachate in this region appears limited. A critical

https://doi.org/10.60787/ijtec.vol1no1.34

finding is the containment of the leachate within the upper layers due to the presence of lateritic clay, which is highly impermeable and restricts vertical migration. This containment effect limits the infiltration of contaminants into deeper groundwater-bearing formations. The presence of lateritic clay is confirmed by the low-resistivity zones observed at shallow to intermediate depths.

The presence of low-resistivity zones in the topsoil and near-surface layers confirms the accumulation of leachate in the unsaturated zone. The impermeable nature of the lateritic clay serves a protective function by limiting the downward migration of the contaminants into deeper aquifer zones. However, the high porosity and permeability of the surface soil suggest that the area is vulnerable to further leachate infiltration during rainfall or surface runoff events. The identification of a leachate plume, indicated by the blue coloration in the resistivity model, underscores the need for proactive environmental monitoring and management around the dumpsite. Although the deeper aquifers appear protected for now, continuous contamination of the topsoil could eventually lead to lateral spread or breakthrough into lower strata through fractures or weaknesses in the clay layer. Therefore, the results highlight the urgent need for landfill containment measures and regular groundwater quality assessments to safeguard public health and prevent long-term environmental degradation.

Similarly, resistivity data from transverse 2 were also employed to generate the 2-D dipole-dipole profile maps presented in Figures 5 and 6.

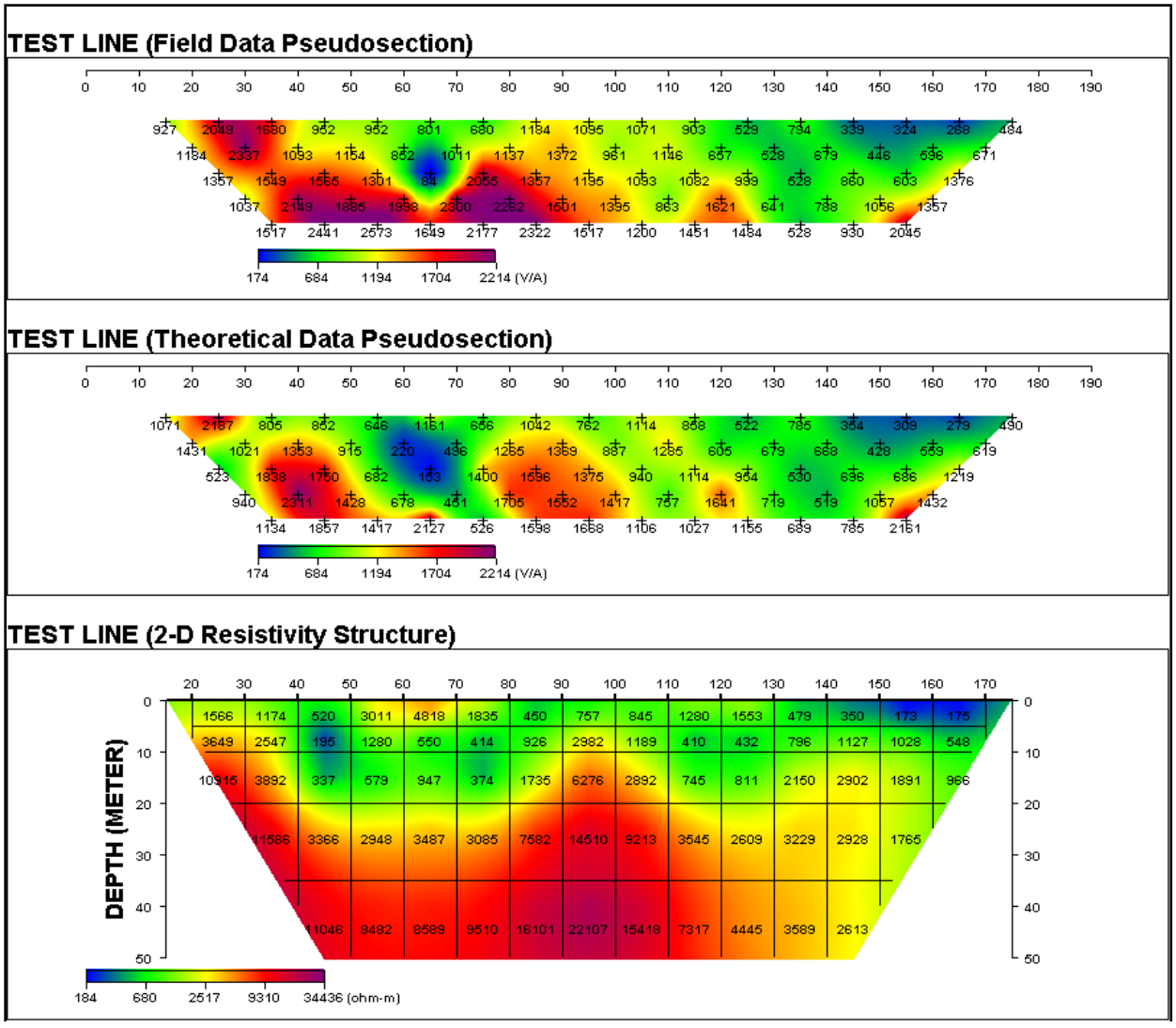

Figure 5: Dipro Inversion based on FEM Modeling

https://doi.org/10.60787/ijtec.vol1no1.34

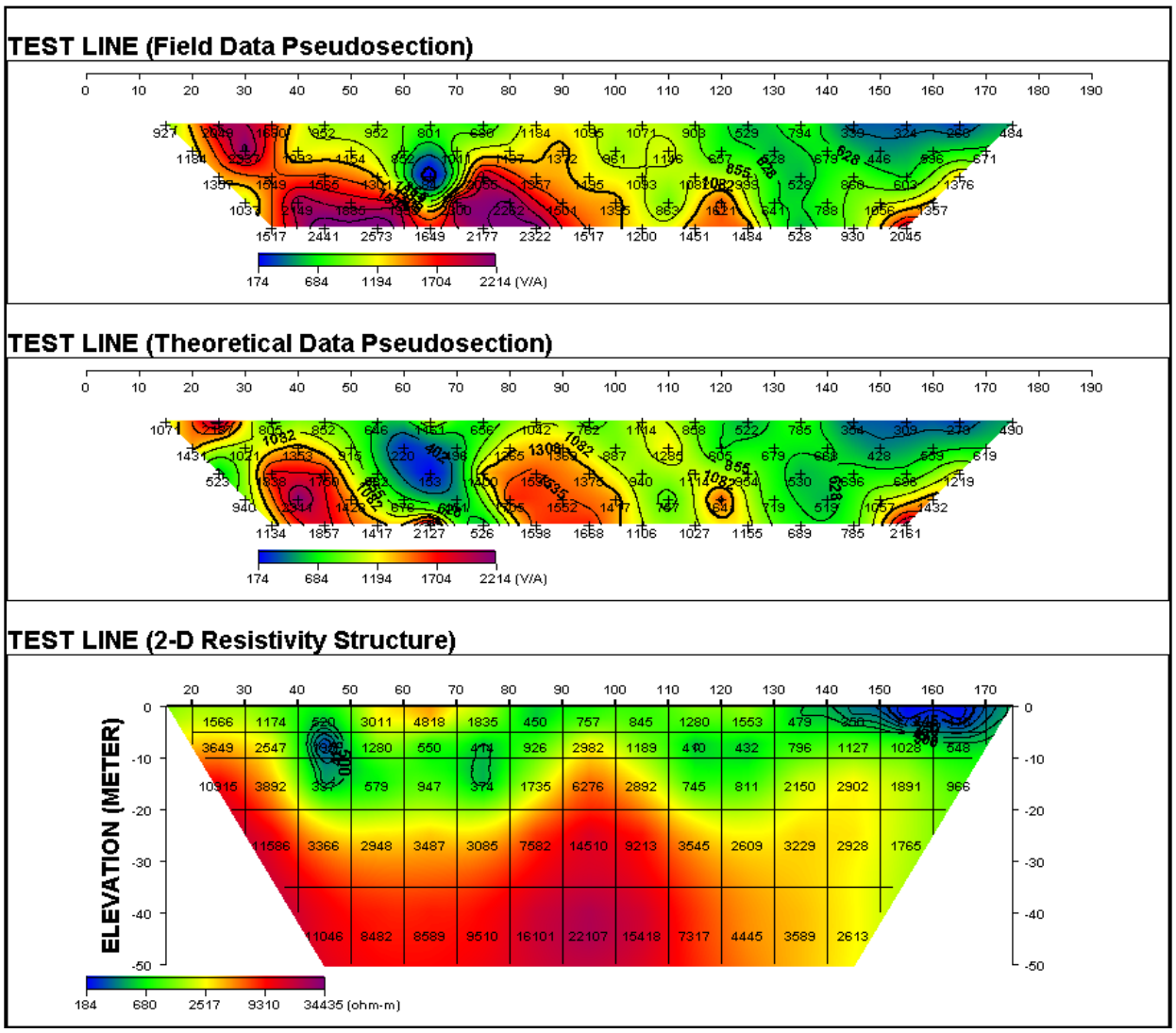

Figure 6: Dipro Inversion based on FEM Modeling with contours

The 2-D resistivity structure presented in Figures 5 and 6 illustrates subsurface variations across the second transverse line in the study area. Surface resistivity values range from 184 Ωm to 548 Ωm and generally increase with depth, indicating changes in lithology and moisture content.

At a horizontal distance of 40 to 50 meters and at a depth of 10 to 20 meters, a low resistivity zone ranging from 184 Ωm to 337 Ωm was detected. This resistivity range is consistent with zones of elevated moisture and dissolved ions, pointing to the presence of leachate. Another leachate-contaminated zone was observed between 60 and 70 meters horizontally and 10 to 20 meters in depth, with resistivity values of 374 Ωm to 414 Ωm. Additionally, at a horizontal distance of 140 to 170 meters and a shallow depth of 0 to 10 meters, resistivity values between 374 Ωm and 548 Ωm indicate further surface leachate accumulation. The topsoil between 140 and 170 meters shows significant contamination by leachate. However, as in the first transverse line, the infiltration of leachate into the deeper layers appears limited. This is attributed to the presence of lateritic clay, a highly impermeable layer that acts as a barrier to vertical contaminant migration.

The presence of leachate in both shallow and intermediate depths, particularly in areas with resistivity values below 400 Ωm, suggests active contaminant infiltration from surface waste materials. The distribution of low resistivity zones points to areas where subsurface contamination is most likely occurring, and these may correspond with poorly managed or unlined waste disposal zones. Although the impermeable lateritic layer currently limits the downward migration of contaminants, the ongoing surface accumulation of leachate poses long-term risks. Over time, leachate may find pathways through

https://doi.org/10.60787/ijtec.vol1no1.34

fractures or weathered zones, particularly under persistent hydraulic pressure during the rainy season. These findings reinforce the need for robust waste management practices, including proper landfill lining, surface runoff control, and continuous monitoring of soil and groundwater quality. The interpretation also highlights critical zones that should be prioritized for remediation or risk mitigation to prevent further environmental degradation and groundwater contamination.

3.2. Soil Analysis and Geospatial Interpolation

The X-ray fluorescence (XRF) spectrometric analysis provided quantitative data on the elemental composition of the soil samples collected around the dumpsite. The results revealed the concentrations of various heavy metals and trace elements in each sample, offering critical insight into potential contamination levels across the study area. To better understand the spatial distribution and intensity of each detected element, Inverse Distance Weighting (IDW) interpolation was applied using the elemental concentration data. The resulting IDW maps (Figures 7 - 14) below visually illustrate the spatial variability of metal concentrations across the sampled locations

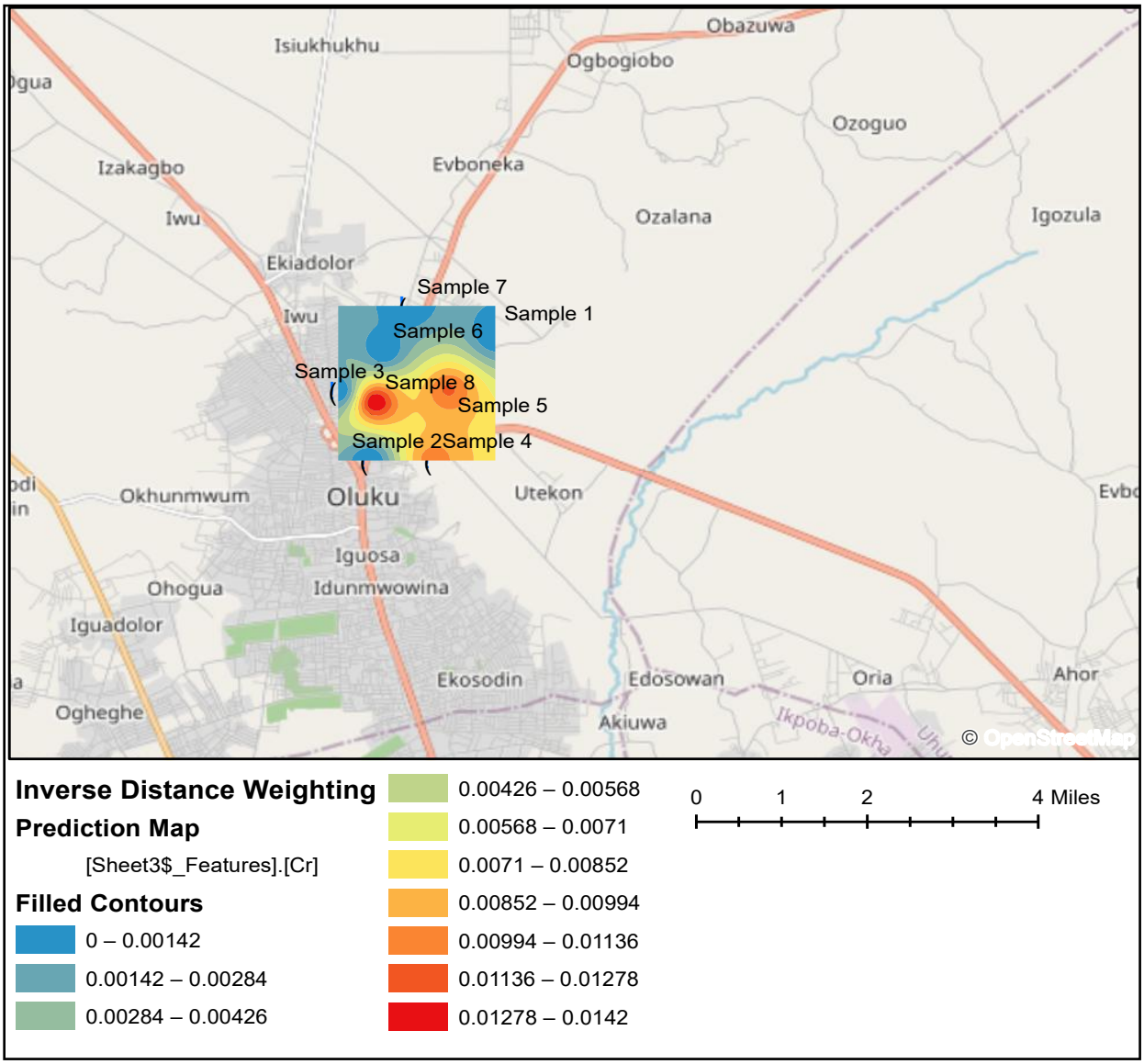

Figure 7: Spatial distribution of Chromium in soil (mg/gram)

https://doi.org/10.60787/ijtec.vol1no1.34

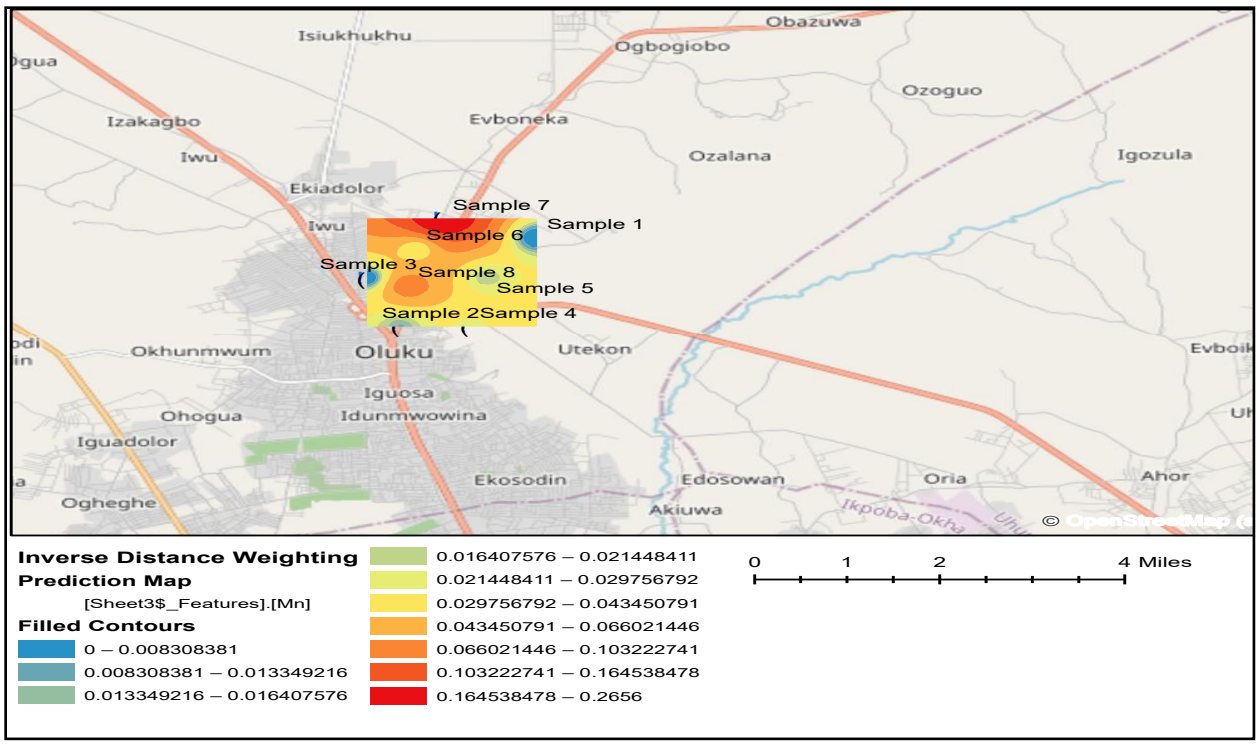

Figure 8: Spatial distribution of Manganese in soil (mg/gram)

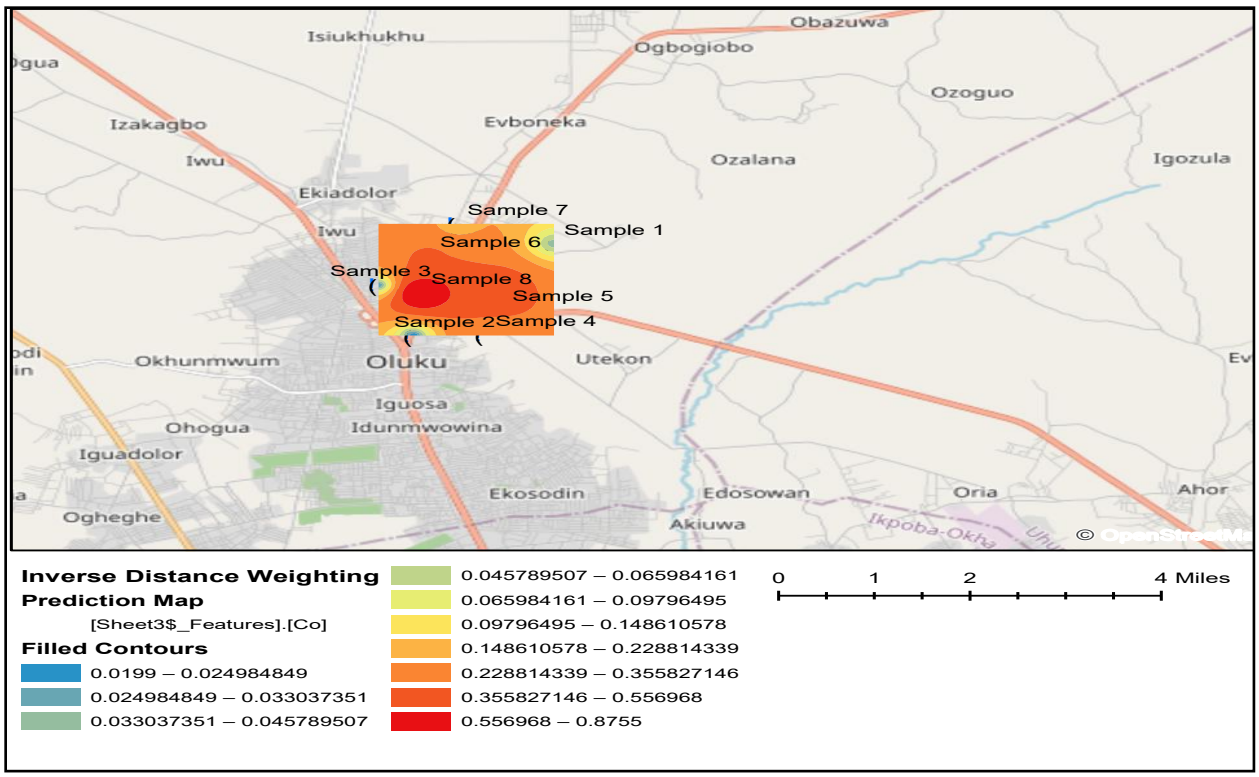

Figure 9: Spatial distribution of Cobalt in soil (mg/gram)

https://doi.org/10.60787/ijtec.vol1no1.34

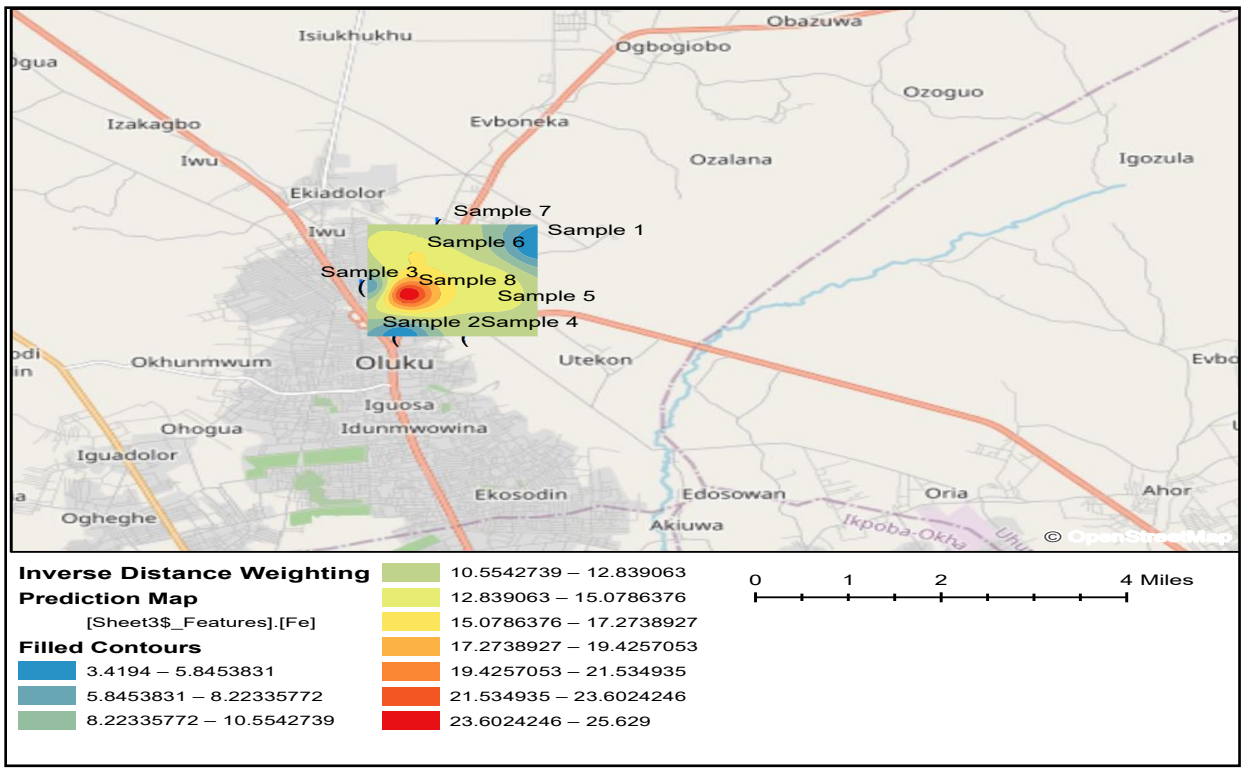

Figure 10: Spatial distribution of Iron in soil (mg/gram)

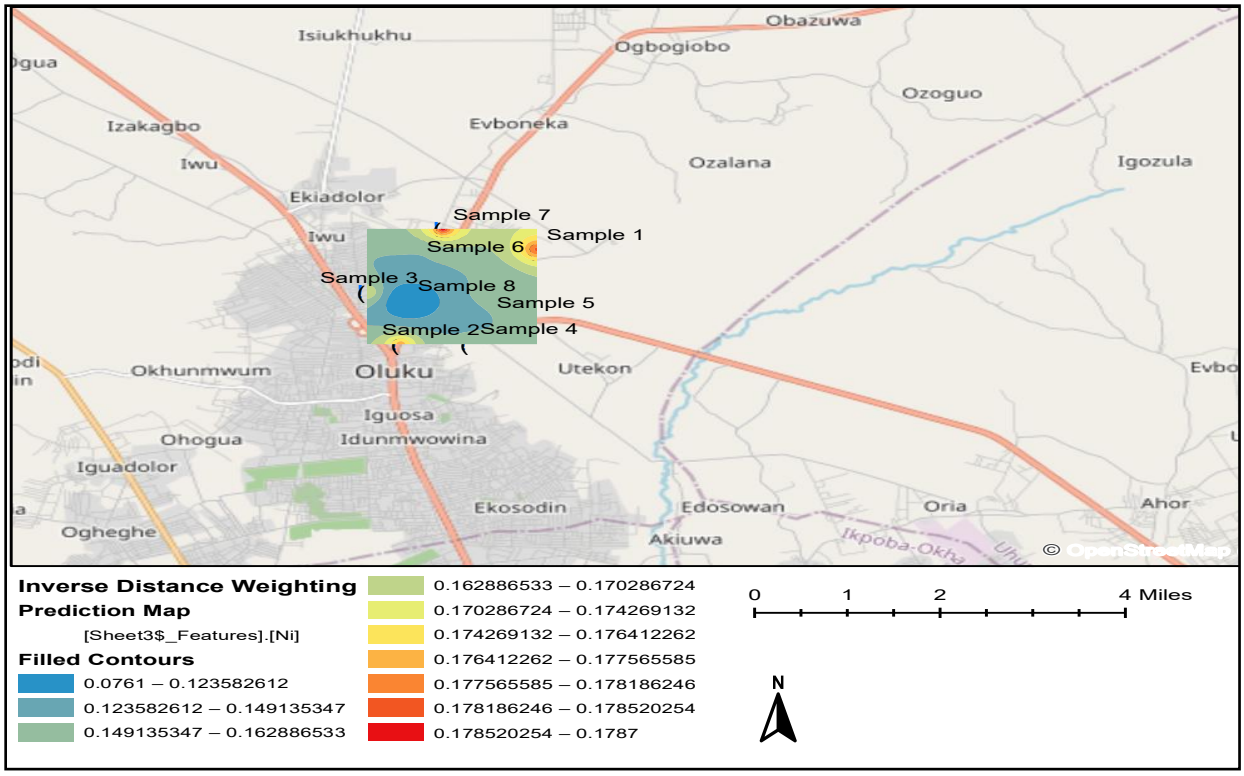

Figure 11: Spatial distribution of Nickel in soil (mg/gram)

https://doi.org/10.60787/ijtec.vol1no1.34

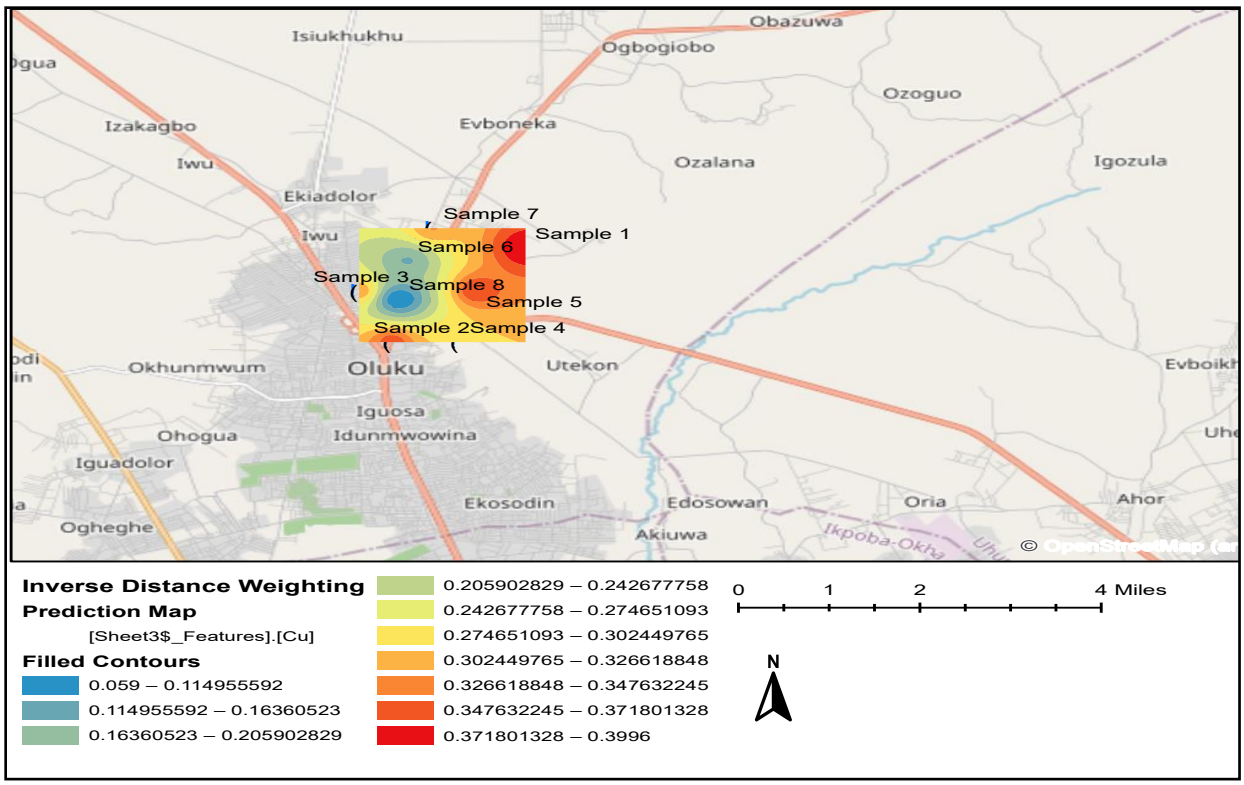

Figure 12: Spatial distribution of Copper in soil (mg/gram)

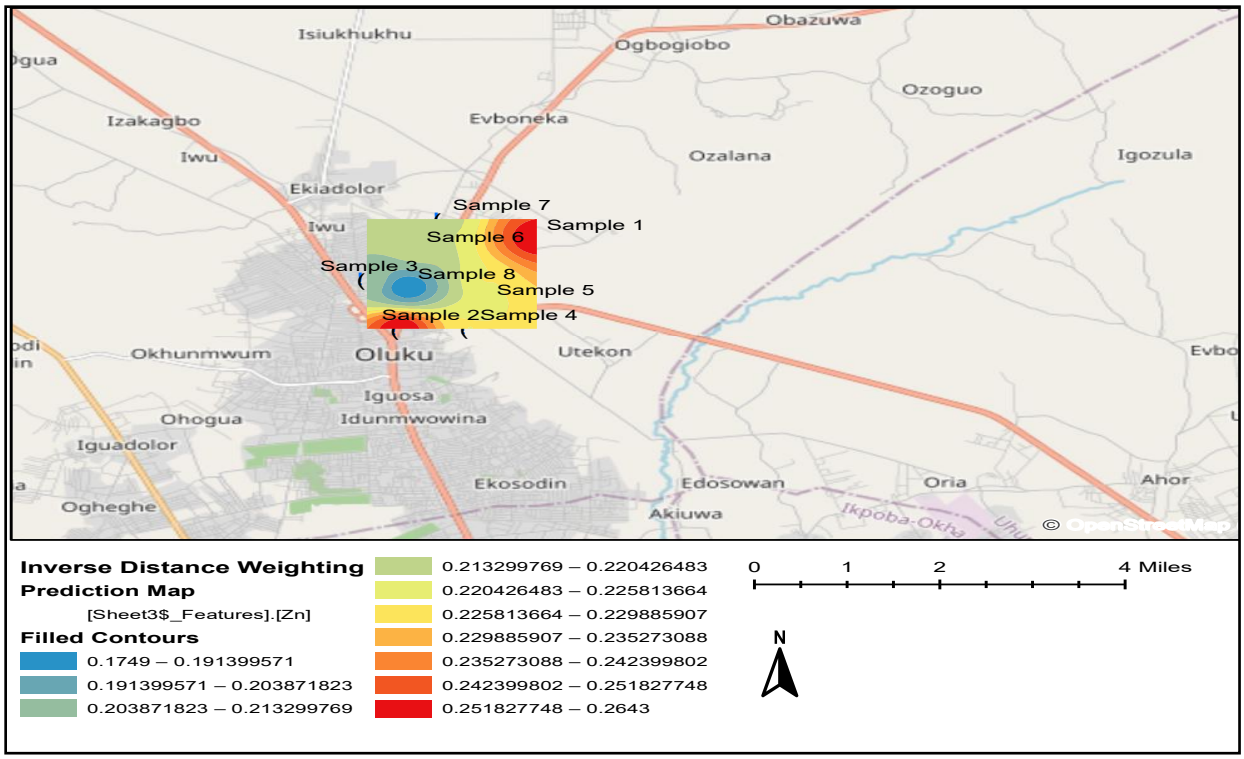

Figure 13: Spatial distribution of Zinc in soil (mg/gram)

https://doi.org/10.60787/ijtec.vol1no1.34

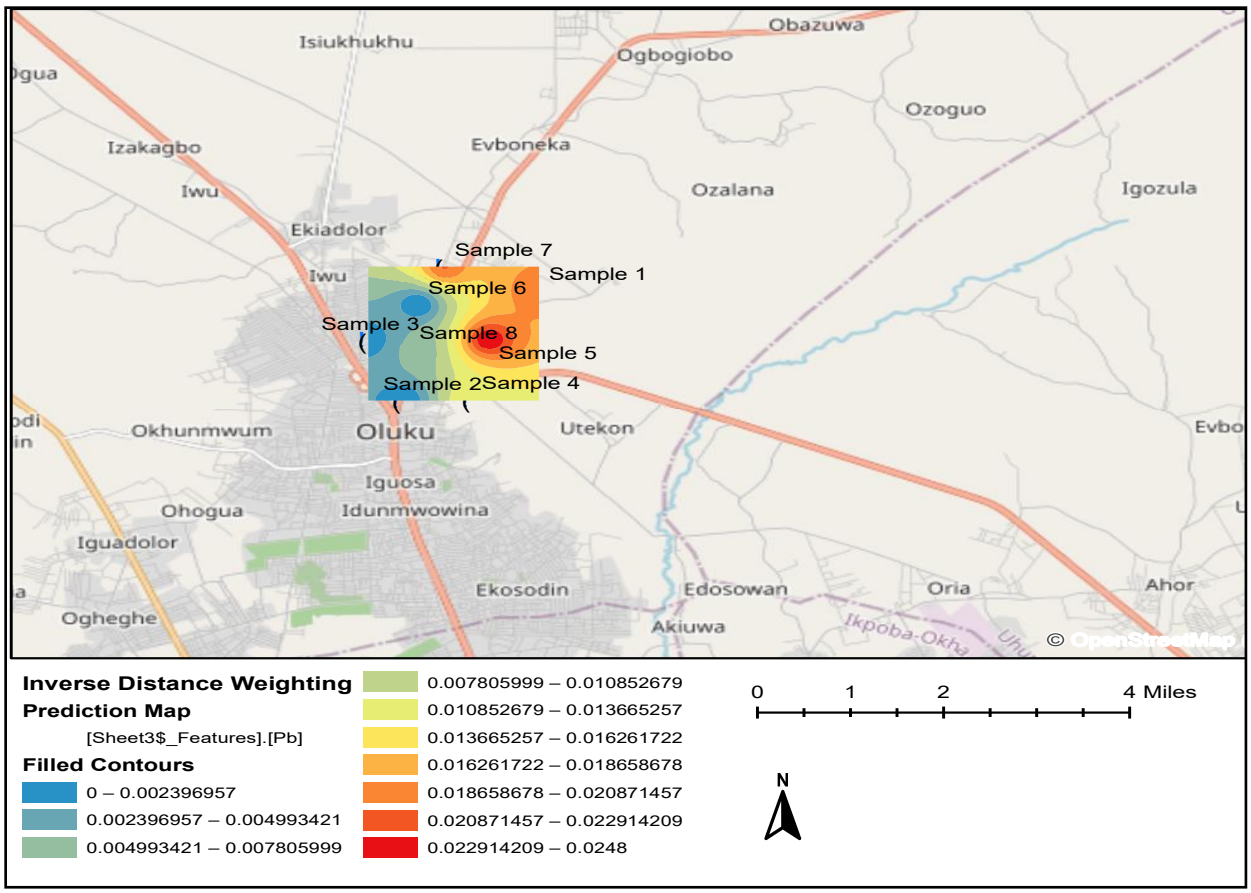

Figure 14: Spatial distribution of Lead in soil (mg/gram)

In these maps, a color gradient was employed, where increasing concentrations of elements are represented by a transition from blue (low concentration) to red (high concentration). This visual representation facilitates the identification of potential contamination hotspots and provides a clearer understanding of the dispersion patterns of individual metals in the soil.

Table 4: Threshold and permissible limits for heavy metals in soil (Source: Adagunodo et al. [10])

Variables	Threshold limit (mg/kg)	Permissible limit (mg/kg)	Mean of Present Study(mg/kg)
Cu	100	50.0 (er)	288.12
Pb	60	200.0 (hr)	10.638
Cr	100	200.0 (er)	4.563
Zn	200	250.0 (er)	225.5
Ni	50	100.0 (er)	153.6
Co	20	100.0 (er)	286.35
As	5.0	50.0 (er)	0.00
Cd	1.0	10.0 (er)	0.1125
Sb	2.0	10.0 (hr)	5469.663
V	100.0	150.0 (er)	2.1625

NB: The risk associated with higher concentrations greater than the permissible limits are grouped into ecological risk (er) and health risk (hr).

https://doi.org/10.60787/ijtec.vol1no1.34

When the measured concentrations were compared against the maximum permissible limits shown in table 4 above, it was observed that the majority of the analyzed elements remained within safe environmental thresholds. This suggests that, overall, the soil environment in the vicinity of the dumpsite has not yet reached a critical level of contamination for most elements. However, Antimony (Sb), Nickel (Ni), Cobalt (Co), and Copper (Cu) were noted to have concentrations that greatly exceeded their permissible limit values. This elevation raises environmental concern, as it may indicate the onset of elemental accumulation in the soil possibly resulting from long-term waste deposition or leachate seepage from the dumpsite. Continued accumulation without intervention could lead to future environmental degradation and potential harm to surrounding ecosystems and human health.

The detection of elevated levels of Sb, Ni, Co, and Cu, highlights the importance of continuous monitoring of soil quality in and around the dumpsite. Proactive soil management and periodic XRF assessments should be conducted to track any progressive increases in metal concentrations. In particular, attention should be given to anthropogenic activities contributing to the elevated levels of these metals, such as improper disposal of metallic waste or corrosion of metal-based materials within the dumpsite. Furthermore, areas showing higher concentrations in the IDW maps should be prioritized for remediation or risk mitigation strategies to prevent potential leaching into groundwater or uptake by plants, especially if the site is close to agricultural zones or water sources.

3.3. Limitations and Future Work

The use of Inverse Distance Weighting (IDW) for spatial interpolation assumes that contamination decreases smoothly with distance from the source, which may not always reflect complex subsurface flow patterns or localized anomalies. This could oversimplify the spatial distribution of contaminants. Future research will focus on using machine learning algorithms to determine the spatial distribution of elemental composition of the soil.

4.0. CONCLUSION

This study successfully integrated geophysical, geochemical, and spatial analytical methods to assess the extent of subsurface contamination and elemental distribution around the dumpsite environment. The 2-D resistivity imaging revealed the presence and spatial spread of leachate plumes. The leachate migration from the topsoil to subsoil stop at 10m depth in most area of study because of the presences of impermeable clay layer. The direction of flow of the leachate is in the Northwest direction of dumpsite. At this depth of contamination however, the groundwater is still safe, because of the impermeable layer of clay which prevent seepage of leachate into the aquifer, which is located at a much farther depth in the Benin formation.

Furthermore, elemental analysis using XRF spectroscopy offered critical insight into the concentration and distribution of various metals within the soil. While most elemental concentrations remained within permissible limits, great exceedances of Antimony (Sb), Nickel (Ni), Cobalt (Co), and Copper (Cu) with mean values of 5469.663 mg/kg, 153.6 mg/kg, 286.35 mg/kg, and 288.12 mg/kg respectively signals the onset of possible contamination trends that warrant further monitoring. The spatial interpolation maps reinforced these findings, identifying localized hotspots that could pose future environmental and health risks if unmanaged.

Collectively, the study underscores the vulnerability of shallow subsurface environments to leachate intrusion from waste disposal activities, while also highlighting the value of integrating geophysical and chemical data for environmental assessment. These findings are crucial for informing sustainable waste management practices, guiding remediation efforts, and supporting policy development to protect soil and groundwater resources.

Conflict of Interest

The authors declare that there is no conflict of interest regarding the publication of this paper.

Authors' Contributions: Ilaboya, I. R. conceptualized the study and supervised the project. Enodiana, O. M. conducted the data collection. Both authors reviewed and approved the final manuscript.

Author's Declaration

The authors affirm that the content of this manuscript is original, has not been published elsewhere, and is not under consideration for publication in any other journal. The authors accept full responsibility for the integrity and accuracy of all data and interpretations presented herein.

Acknowledgments

The authors also wish to disclose the use of ChatGPT for grammar refinement and language polishing, which contributed to improving the manuscript's clarity and readability. Additionally, Adobe Illustrator was utilized for the creation of the graphical abstract. These tools were used exclusively for editorial and illustrative

https://doi.org/10.60787/ijtec.vol1no1.34

purposes and did not influence the research methodology, analysis, or interpretation of results.

References

[1] Ige, O. O., Owolabi, A. T., Olabode, O. F., & Obasaju, D. O. (2022). Groundwater quality evaluation: A case study of Igando waste dumpsite, southwestern Nigeria. Applied Water Science, 12(4), 1-15. https://doi.org/10.1007/s13201-022-01601-x

[2] Adeoye, A. S., Ige, O. O., Talabi, A. O., & Oyebamiji, A. (2023). Geophysical evaluation of the impact of solid waste dumpsite on the groundwater in Ilokun, Ado-Ekiti, southwestern Nigeria. Asian Journal of Geological Research, 6(2), 93-103.

[3] Olatunji, S., & Fauzan, A. (2023). Geophysical assessment of groundwater contaminations from leachate intrusion in Amoyo dumpsite. Journal of Fundamental and Applied Sciences, 14(1), 181-209. https://doi.org/10.4314/jfas.v14i1.10

[4] Ojo, A., Oyelami, A., & Babafemi, E. (2021). Groundwater quality assessment of abandoned dumpsite in Osogbo suburb, Nigeria: Hydrogeological and geophysical condition six years after initial study. Journal of Applied Science and Environmental Management, 25(7), 1213-1219. https://doi.org/10.4314/jasem.v25i7.17

[5] Joe-Ukairo, A., & Oni, A. G. (2018). Geophysical and hydro-chemical investigations of Oke Asunle dumpsite in Ile-Ife, southwestern Nigeria for subsoil and surface water pollution. Journal of Health and Pollution, 8(20), Article 181209. https://doi.org/10.5696/2156-9614-8.20.181209

[6] Ferreira, C. S., Adama-Ajonye, O., Ikenna, A. E., & Kalantari, Z. (2023). Groundwater quality in the vicinity of a dumpsite in Lagos metropolis, Nigeria. Geography and Sustainability, 4(4), 379-390. https://doi.org/10.1016/j.geosus.2023.09.005

[7] Udosen, N. I. (2021). Geo-electrical modeling of leachate contamination at a major waste disposal site in south-eastern Nigeria. Modeling Earth Systems and Environment, 8(1), 847-856. https://doi.org/10.1007/s40808-021-01120-9

[8] Zaini, M. S. I., Hasan, M., & Zolkepli, M. F. (2021). Urban landfills investigation for leachate assessment using electrical resistivity imaging in Johor, Malaysia. Environmental Challenges, 6, Article 100415. https://doi.org/10.1016/j.envc.2021.100415

[9] United States Environmental Protection Agency. (2016). Resistivity methods. https://www.epa.gov

[10] Adagunodo, T., Sunmonu, L., & Emetere, M. (2018). Heavy metals' data in soils for agricultural activities. Data in Brief, 18, 1847-1855. https://doi.org/10.1016/j.dib.2018.04.115